Received: 7 September 2023 | Revised: 1 April 2024 | Accepted: 2 May 2024

DOI: 10.1002/hyp.15170

RESEARCH ARTICLE

WILEY

Dissolving the mystery of subsurface controls on snowmelt–discharge dynamics in karst mountain watersheds using hydrologic timeseries

Daniel Thurber[1,2] | Belize Lane[1] | Tianfang Xu[3] | Bethany T. Neilson[1]

[1]Department of Civil and Environmental Engineering, Utah State University, Logan, Utah, USA

[2]WSP USA, Tucson, Arizona, USA

[3]School of Sustainable Engineering and the Built Environment, Arizona State University, Tempe, Arizona, USA

Correspondence
Belize Lane, Department of Civil and Environmental Engineering, Utah State University, Logan, UT, USA.
Email: belize.lane@usu.edu

Funding information
U.S. National Science Foundation, Grant/Award Numbers: 2044051, 2043363; Utah Water Research Laboratory, Utah State University

Abstract

Streamflow generation in mountain watersheds is strongly influenced by snow accumulation and melt as well as groundwater connectivity. In mountainous regions with limestone and dolomite geology, bedrock formations can host karst aquifers, which play a significant role in snowmelt–discharge dynamics. However, mapping complex karst features and the resulting surface-groundwater exchanges at large scales remains infeasible. In this study, timeseries analysis of continuous discharge and specific conductance measurements were combined with gridded snowmelt predictions to characterize seasonal streamflow response and evaluate dominant watershed controls across 12 monitoring sites in a karstified 554 km^2 watershed in northern Utah, USA. Immense surface water hydrologic variability across subcatchments, years and seasons was linked to geologic controls on groundwater dynamics. Unlike many mountain watersheds, the variability between subcatchments could not be well described by typical watershed properties, including elevation or surficial geology. To fill this gap, a conceptual framework was proposed to characterize subsurface controls on snowmelt–discharge dynamics in karst mountain watersheds in terms of conduit flow direction, aquifer storage capacity and connectivity. This framework requires only readily measured surface water and climatic data from nested monitoring sites and was applied to the study watershed to demonstrate its applicability for evaluating dominant controls and climate sensitivity.

KEYWORDS
aquifer, geology, groundwater, hydrologic connectivity, karst, karst hydrology, snowmelt, storage, surface-groundwater exchange, timeseries analysis

1 | INTRODUCTION

In continental mountain regions, snow accumulation and melt are dominant controls on streamflow and water availability to downstream users and aquatic ecosystems (Barnhart et al., 2016; Brooks et al., 2021; Horner et al., 2020). The underlying geology of mountain watersheds also influences snowmelt–discharge dynamics based on the importance of surface and subsurface flow pathways (Carlier et al., 2018; Jefferson et al., 2008; Tague & Grant, 2009), and the relative contributions and residence times along different flow paths can impact streamflow patterns and climate sensitivity. Reduced seasonal snow storage with warming temperatures is further increasing the

importance of groundwater contributions to streamflow (Arnoux et al., 2021; IPCC, 2015). In karst-influenced mountain watersheds in particular, discharge can respond quickly to snowmelt and rain via karst conduits (Jeannin & Sauter, 1998; Sauter, 1992), and climate change is expected to alter the relative flow contributions and timing of karst conduit, matrix and overland flow to streams. Godsey et al. (2014) suggested that low streamflows in systems with significant bedrock aquifer storage may be buffered and less sensitive to interannual snowpack variability than watersheds with low-porosity crystalline bedrock. Segura et al. (2019) and Hellwig et al. (2020) also reported short-term buffering of drought year summer baseflows in areas underlain by porous geology. Liu et al. (2021) found that karst controls between 65% and 93% of the total streamflow sensitivity to precipitation across watersheds. However, the climate sensitivity of karst-influenced watersheds remains unclear due to the combined influence of overland flow, fast conduit flow and slower matrix-dominated flow pathways. No framework has been widely adopted for characterizing these systems with respect to groundwater controls on streamflow, and recent work suggests varied sensitivity to interannual changes in snow accumulation and melt volumes (Hartmann et al., 2017; Liu et al., 2021). Understanding dominant flow pathways and sources in karst mountain watersheds is critical for predicting streamflow trends and assessing hydrologic vulnerability to climate change.

Karst-carbonate aquifers pose a particular challenge for understanding the role of groundwater on streamflow response and climate sensitivity due to their heterogeneous subsurface flow paths that can store and transport large volumes of water. Karst conduits develop preferentially along bedding planes, vaults or conjugate fracture networks (Ford & Williams, 2007). Conduits along bedding planes provide for groundwater conveyance based on dip direction while conduits along structural fractures can facilitate vertical groundwater movement (Hartmann et al., 2014; White, 2002). High-volume conduit pathways may result in groundwater exchanges between adjacent watersheds (Cochand et al., 2019; Hartmann et al., 2014). This karst "piracy" has been repeatedly confirmed through conservative tracer studies of spring recharge areas (Goldscheider et al., 2008; Spangler, 2001). Complex conduit geometry can also form subsurface storage reservoirs (Jódar et al., 2020) feeding multiple spring outlets with asynchronous responses. Ongoing conduit–matrix storage exchanges also have the potential to shift flow direction on seasonal timescales (Hartmann et al., 2014), with water moving from conduits to matrix storage during the wet season and then back into conduits during the dry season. Because of the abundance of limestone and dolomite, much of the research on mountain karst hydrology is from the European Alps (Somers & McKenzie, 2020), with an emphasis on spring outlets that serve as drinking water sources (Baudement et al., 2017; Jódar et al., 2020). However, the heterogeneity of karst watersheds and the monitoring and modelling challenges associated with characterizing aquifer structure and dynamics continue to limit our understanding of these unique systems. Liu et al. (2021) found that karst-influenced watersheds exhibited both enhanced and reduced streamflow relative to hydrologic simulations in the absence of karst, depending on karst features and aquifer properties.

Numerous modelling approaches have been used to represent the complex subsurface dynamics of karst aquifers, but the combined effects of surface and subsurface flow pathways on streamflow remain poorly understood. Numerical models have predicted karst spring discharge as a function of precipitation or snowmelt inputs. Model structure typically involves reservoirs for conduit, matrix and near-surface "epikarst" storage (Baudement et al., 2017; Chen et al., 2018). However, such studies are resource intensive and geographically constrained, as discussed in Hartmann et al. (2014) and Xu et al. (2018). Karst aquifers are broadly conceptualized as having two distinct flow pathways: karst conduits characterized by high velocity flow and short residence times (less than 30 days) and non-karst matrix flow through porous media or highly fractured bedrock with residence times of several years or more (Hartmann et al., 2014). Some recent studies have expanded on this simple dichotomy to include flow pathways with intermediate residence times. For example, Wang et al. (2019) used multiple Gaussian analysis of frequency distributions to propose as many as eight distinct groundwater pathways. In reality, karst mountain streamflow represents the combined inputs from distinct residence time flow pathways with differing contributions across seasons, years and subcatchments.

Because the specific structure of karst aquifers often cannot be adequately physically observed or modelled, analyses of measurable variables such as streamflow, stream water quality and snowmelt provide an alternative approach to characterize these systems. During baseflow (generally late summer through winter), the conduits are largely drained and the fraction derived from fractured matrix and epikarst increases. During the snowmelt period, conduit flow is a much larger component of the spring flow and thus the river flow, along with overland runoff contributions, as observed in northern Utah (Neilson et al., 2018). These alternate flow pathways are manifested as diverse streamflow and chemical responses to similar precipitation inputs (Chang et al., 2021; Jódar et al., 2020; Neilson et al., 2018). Neilson et al. (2018, 2021) demonstrated how such variability in chemical responses can be used in mass and flow balances to quantify groundwater exchanges in nested karst mountain subcatchments. However, such approaches rely on intensive water quality monitoring and laboratory analysis in addition to streamflow data, limiting its broad applicability.

1.1 | Study objectives

This study used measurable hydrologic and climate data to evaluate seasonal flow pathways and characterize dominant subsurface controls in subcatchments spanning a large topographic gradient. Specifically, we compared snowmelt, streamflow and specific conductance (SpC) patterns between subcatchments, seasons and years relative to the watershed outlet, and evaluated established relationships between hydrologic metrics and watershed properties. Finally, we proposed a new conceptual model of subsurface controls on streamflow dynamics in karst mountain watersheds terms of (1) inter-basin exchange directions of conduit flow, (2) groundwater storage capacity and (3) the connectivity of storage to outflow springs.

2 | MATERIALS AND METHODS

2.1 | Study area

This study focused on the semi-arid Logan River watershed in northern Utah, USA, with elevations ranging from 1426 to 3034 m.a.s.l. and a drainage area of 554 km^2 (Figure 1a). This watershed includes several nested, intensively monitored subcatchments spanning a range of elevations and karstification (Table 1, Neilson et al., 2021) and has been the subject of many hydrogeology monitoring and modelling studies, summarized in Supplemental Materials (Bahr, 2016; Lachmar et al., 2021; Neilson et al., 2018; Spangler, 2001, 2011). Average annual precipitation ranges from 45 to 125 cm with the majority falling as snow. Total snow accumulation (max snow water equivalent [SWE]) over the study period (2015–2022) ranged from 67 to 137 cm, observed at the Tony Grove Lake SNOTEL station. The Logan River hydrology is snowmelt-dominated, with peak flows in the spring, low flows spanning late summer through winter and an annual average streamflow of 6.5 m^3/s at the watershed outlet (FD [First Dam] in Figure 1a). Dewitt Springs serves as the primary drinking water source for the nearby city of Logan, Utah.

The bedrock geology of the watershed (Figure S1a) consists of primarily Palaeozoic-age limestone and dolomite with karst topography marked by sinkholes and fractures that feed subsurface drainage systems intercepted by interbedded siliciclastic units (Bahr, 2016; Dover, 2007; Spangler, 2001). Dominant geologic structures include the northeast-southwest trending Logan Peak Syncline near the western watershed boundary and normal faults and grabens to the east, with strata throughout the watershed dipping to the west (Dover, 2007; Figures 1a and S1). In some areas, Palaeozoic carbonate strata are overlain unconformably by crudely stratified conglomerates and siltstones of the Wasatch Formation (Eocene).

2.2 | Data inputs and processing

Timeseries of daily average streamflow measurements and simulated combined snowmelt and rainfall inputs were evaluated across sites and water years during defined baseflow, snowmelt and recession periods. These timeseries were used to calculate a suite of seasonal hydrologic metrics that were plotted against watershed properties and hydro-climate conditions to assess potential streamflow controls. Geospatial and timeseries datasets were assembled and processed to extract relevant information as described below. Throughout the paper, year assignments refer to the water year (WY).

2.2.1 | Simulated surface water input timeseries

Combined snowmelt and rainfall timeseries (surface water inputs, or SWIT) were aggregated from spatially distributed (100-m) model simulation results for the Logan River basin (Tyson et al., 2023; Xu

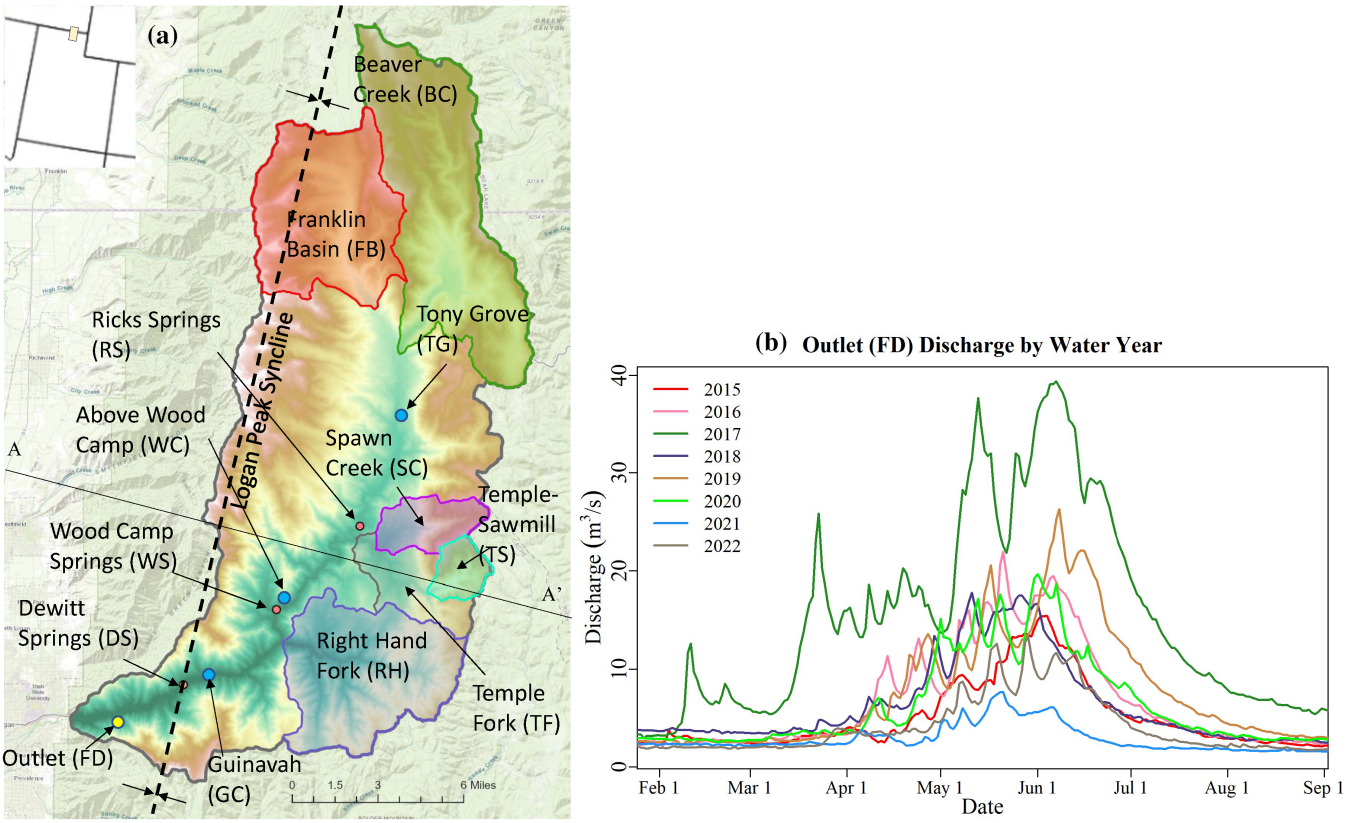

FIGURE 1 (a) Study area map including nested subcatchment and spring locations, and (b) daily average streamflow at the watershed outlet by water year through study period. The A to A' geologic cross section indicated in (a) is provided in Figure S1.

TABLE 1 Name, drainage area, median elevation, and areal percentage of surface karst (Weary & Doctor, 2014) of each monitoring site where applicable.

Site code	Site name	Area (km^2)	Median elevation (m)	Surface karst (%)
FB	Franklin Basin	65.9	2526	65
TG	Tony Grove*	278.0	2488	50
BC	Beaver Creek	103.4	2491	94
TF	Temple Fork	41.4	2260	63
RH	Right Hand Fork	65.20	2088	46
RS	Ricks Spring	NA (spring)	1785 (outlet elev)	NA
TS	Temple-Sawmill	8.61	2417	99
SC	Spawn Creek	14.7	2299	46
WC	Above Wood Camp*	403.9	2435	70
GC	Guinavah Campground*	520.8	2348	69
WS	Wood Camp Hollow Spring	NA (spring)	1629 (outlet elev)	NA
FD	First Dam (Outlet)*	554.0	2336	71

Abbreviation: NA, not applicable.
*Monitoring site on the mainstem of the Logan River.

et al., 2022) based on the Utah Energy Balance (UEB) snow model for WYs 1989–2022 at an hourly timestep. To calculate the hydrologic metrics described below, simulated gridded SWIT values were averaged across each subcatchment, then summed across timesteps to provide subcatchment-wide daily SWIT estimates.

The UEB model simulates the mass and energy balances of the snowpack both on the ground and intercepted by canopy (Tarboton & Luce, 1996). The model was driven by NLDAS-2 forcing downscaled to 100-m resolution using orographic adjustment; and further bias-corrected using observations at six SNOTEL stations within the modelled area (Xu et al., 2022). As a result, simulated SWIT is subject to uncertainties from forcing, downscaling and precipitation undercatch error (Tyson et al., 2023; Xu et al., 2022).

2.2.2 | Streamflow and SpC timeseries

Logan River Observatory stations along the mainstem (TG [Tony Grove], WC [Wood Camp], GC [Guinavah Campground]), in six tributary subcatchments (FB [Franklin Basin], BC [Beaver Creek], RH [Right Hand Fork], SC [Spawn Creek], TF [Temple Fork], TS [Temple-Sawmill]), and at two springs (RS [Ricks Spring], WS [Wood Camp Hollow Spring]) provided the bulk of flow and SpC data (referenced to 25°C) used in the analyses over the available time periods (Figure 1a; Table 1). The U.S. Geological Survey (USGS) operates an additional gauge at the mouth of Logan Canyon (FD, USGS 10109000), providing discharge for WY 1987–2021. Just upstream from FD, a diversion canal withdraws up to 2.3 m^3/s from the river during the irrigation season (starting around April 15) that can alter flow at FD. All monitoring stations record data at 15-min intervals and stage height observations were converted to discharge via rating curves developed by the Logan River Observatory or USGS. Details on field monitoring, QA/QC protocols and links to public datasets are available in Neilson et al. (2021).

All aquatic timeseries data were smoothed through daily averaging, and data gaps were filled using linear interpolation. During the high-flow season (March–July), filled data gaps were limited to periods of 1 to 5 days. Extended data gaps occurred in winter months (November–February) due to instrument icing. Interpolation of discharge during this period was only used for runoff ratio calculations. Field observations and recorded discharge at other stations show minimal streamflow variability during these cold months. Intervals of data availability for each site are shown in Figure S2. WS has multiple outlets that make direct discharge measurements infeasible. Instead, spring discharge was estimated as the difference in river discharge measured at WC and another gauging location just below the inflow of WS.

2.2.3 | Watershed properties

Several topographic and geologic properties were calculated for each subcatchment (Tables 1 and S1). Drainage areas were delineated using USGS StreamStats v4. Median elevation, median slope and average aspect were calculated using USGS 10-m digital elevation models in ArcGIS Pro v10.7 (Addor et al., 2017). Percentage of karst surface extent was calculated based on the surface extent of carbonate karst layers calculated by Weary and Doctor (2014) (Figure S1c).

2.3 | Data analysis

2.3.1 | WY classification

WYs in the study period (2015–2022) were classified based on the cumulative daily average flow at FD from the start of the snowmelt period to 60 days after the recession start date as wet (>70th percentile), moderate (30th to 70th percentile) or dry (<30th percentile).

Designations were based on the snowmelt period only to remove the potential influence of an elevated snowmelt recession carried over from the previous year.

2.3.2 | Normalized hydrographs

Daily average discharge (Q) for each mainstem and subcatchment site (i.e., all monitoring sites except springs) was then normalized by drainage area (A) (Table 1) using Equation 1 to generate area-normalized streamflow timeseries (Q_A).

$$Q_A = \frac{Q}{A}. \quad (1)$$

Next, because flow at the outlet (FD, Figure 1a) represents the integrated watershed response to precipitation, subcatchment Q_A timeseries were further normalized relative to area-normalized streamflow at the outlet (Q_{AO}), where Q_N is the area-outlet normalized streamflow (Equation 2).

$$Q_N = \frac{Q_A}{Q_{Ao}}. \quad (2)$$

Because the springs did not have definitive recharge areas, spring hydrographs were instead compared with other sites via peak flow normalization. Peak-normalized streamflow timeseries (Q_P) were calculated as daily average streamflow divided by WY maximum daily average flow (Q_{max}) at that site (Equation 3).

$$Q_P = \frac{Q}{Q_{max}}. \quad (3)$$

For each study site, daily average Q, Q_A, Q_N (or Q_P), and SpC were plotted over each WY.

2.3.3 | Annual hydrologic metrics

Using the daily average streamflow and SWIT timeseries, several established annual hydrologic metrics were calculated following past studies on mountain watershed hydrology (e.g., Brooks et al., 2021; Curry & Zwiers, 2018; Deshmukh & Singh, 2016; Patterson et al., 2020) (see full list in Table S2). To facilitate comparison between sites, metrics were reported as ratios relative to the watershed outlet. Because many metrics did not yield clear relationships with watershed properties (see Figure S3), we focus only on relevant metrics below.

The annual start dates of the snowmelt, recession and baseflow periods at each site (Table S3) were expert-determined based on visual assessment of streamflow and SWIT patterns following Patterson et al. (2020). Baseflow period start date was selected as October 1 for all years and sites, and snowmelt period start date was set as the last day of low flow in March or April. The recession period starts on the first day of the final snowmelt-driven hydrograph peak, typically followed by a smooth decay curve. Small discharge spikes during the snowmelt recession were ignored in timing determinations.

The baseflow period was summarized using median baseflow magnitude. The snowmelt period was summarized using annual peak flow (Q_{max}) and the melt runoff ratio, calculated as the ratio of cumulative snowmelt period streamflow to cumulative SWIT. The recession period was quantified using the monthly recession slope, the average hydrograph slope in the first 30 days of the recession period, to reduce sensitivity to short snowmelt or rain events. The annual runoff ratio was calculated as the cumulative WY streamflow to SWIT ratio. Scripts for calculating all metrics are available at https://github.com/danielthurber/thesis. Non-normalized metrics for all years and sites are provided in Table S4.

Finally, scatterplots and linear regression were used to evaluate relationships between subcatchment hydrologic metrics and watershed properties, as detailed in Figure S3.

3 | RESULTS

Annual plots of daily average streamflow at the watershed outlet show peak and average discharge varying by an order of magnitude across years (Figure 1b). WYs 2017 and 2021 were classified as very wet and very dry years, respectively, and other years as wet (2019), moderate (2016, 2020) or dry (2015, 2018 and 2022). These assignments were consistent with those of Xu et al. (2022) and Tyson et al. (2023) based on a longer period of record. Hydrographs and simulated daily SWIT spanning the late baseflow, snowmelt and early recession periods are illustrated in Figures 2 and S4.

Area-normalized hydrographs highlight the distinctive behaviour of different tributary subcatchments and mainstem sites (Figure 3). The spring-fed headwater drainage, FB, had much higher Q_A during the snowmelt and recession periods than other mainstem sites. Snowmelt peak Q_A in FB reached ~10.8 mm/day (Q_N ~3) in WY 2019 and ~3.6 mm/day (Q_N ~5) in WY 2021. Omitting FB, the four mainstem sites (TG, WC, GC and FD) had similar streamflow patterns, with differences largely explained by elevation (Figure 3a) and contributions from major springs. Higher elevation TG and WC both showed muted responses to the annual initial snowmelt event relative to lower elevation GC and FD, but similar Q_A patterns through the remainder of the year. Downstream of the spring contributions, GC Q_A remained slightly higher than other mainstem sites in drier years (2020, 2021). The drop in flow at FD in mid-April 2021 (Figure 3) may be attributable to the start of irrigation diversions, and the rising limb rate and peak flows in all years are likely slightly lower than they would be in the absence of the one upstream withdrawal.

Considering the tributary subcatchments (Figure 3b), TS had much higher Q_A than others because the flow at this location is dominated by a large spring that may capture snowmelt water outside of the catchment, while adjacent SC had a negligible snowmelt response. These two sites combine to generate a moderate snowmelt signal at TF with peak flow timing and Q_A peak magnitude similar to that of the

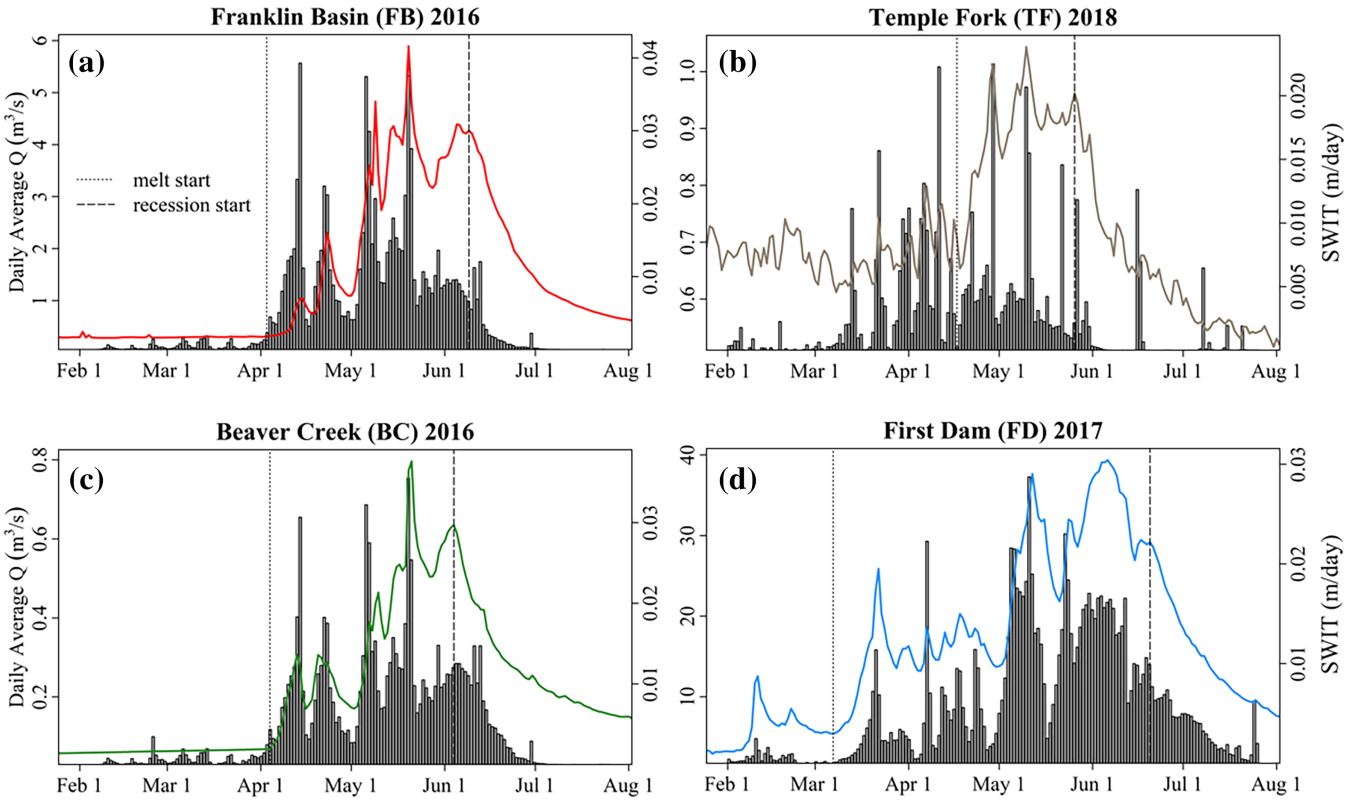

FIGURE 2 Hydrographs and simulated SWIT timeseries (vertical black bars) for selected sites and portions of water years, with the start of the snowmelt period and the start of the recession period indicated as vertical dashed lines. Additional years are shown in Figure S4.

mainstem sites (Figure 3b). A snowmelt pulse was only observed in RH in 2018 and 2019 and occurred in April well before other sites. The Q_A at BC remained very low across seasons and years, with the highest observed Q_A of 2.0 mm/day occurring in mid-June of wet 2019.

A closer look at TF and RH reveals distinct streamflow responses to similar SWIT in 2017 and 2018 (Figure S4). After similar responses to the initial snowmelt pulse, subsequent melting resulted in a clear streamflow response in TF but was almost unnoticeable in RH. Hydrogeologic factors potentially causing this discrepancy are discussed in Section 4, although it could also be attributed to bias in UEB simulation results. Compared with snow accumulation observations at the nearby Temple Fork SNOTEL station, UEB predictions overestimated SWE in WY 2017, thus resulting in simulated snowmelt occurring later than actual, and underestimated SWE in WY 2018 (Xu et al., 2022).

Figure 3c highlights variation in the timing of springs and mainstem seasonal streamflow patterns. In WY 2019 and 2020, RS closely tracked the substantial flow increase at FD in the early snowmelt period (early April) but was hardly perceptible in WC and TS. In contrast, in dry WY 2021 RS had no flow response corresponding to the first snowmelt pulse at FD. Later in the snowmelt period, FB, RS, WS and FD had very similar peak flow timing and recession rates during snowmelt events. Flow initially increased with snowmelt at TS and RS with nearly identical timing at the watershed outlet. The initial response in WC was more delayed, with a moderate response in May and peak flow in June. In drier years, TS reached its seasonal peak in early May and began receding well before, but more slowly than, the other springs and mainstem sites.

The SpC plots (Figure 4) provide additional explanation for the distinct seasonal flow patterns described above. During the snowmelt period, mainstem sites generally exhibited short SpC spikes at the start of the melt period as older water in the matrix is flushed out, then a significant decrease during peak runoff (Figure 4a,c,e), followed by a period of variable and then increasing SpC with a return to baseflow conditions. FB maintained the lowest SpC values throughout the period of record, consistent with the many karst springs observed in the FB subcatchment. The timing of early melt SpC spikes was very similar in FB, TG and WC along the mainstem and in spring-fed RS, although RS had higher values. RH also exhibited a rapid decrease in SpC in the early melt period followed by quick returns to baseflow conditions in wetter years, but these trends were less distinct in drier years. TS exhibited a short increase followed by a long decrease in SpC over the melt period, followed by a rise back to baseflow values. SC had higher SpC than TS, likely because it originates from tufa-depositing springs. SC and TF stayed relatively stable except for a short, but steep, drop during wet-year snowmelt. Finally, BC had very high SpC but trends were erratic, likely due to runoff of salt from winter highway maintenance.

Area-outlet normalized hydrographs (Q_N) highlight differences in flow magnitudes, rise and recession rates relative to the integrated watershed response, represented as a flat line of $Q_N = 1$ in Figure 5.

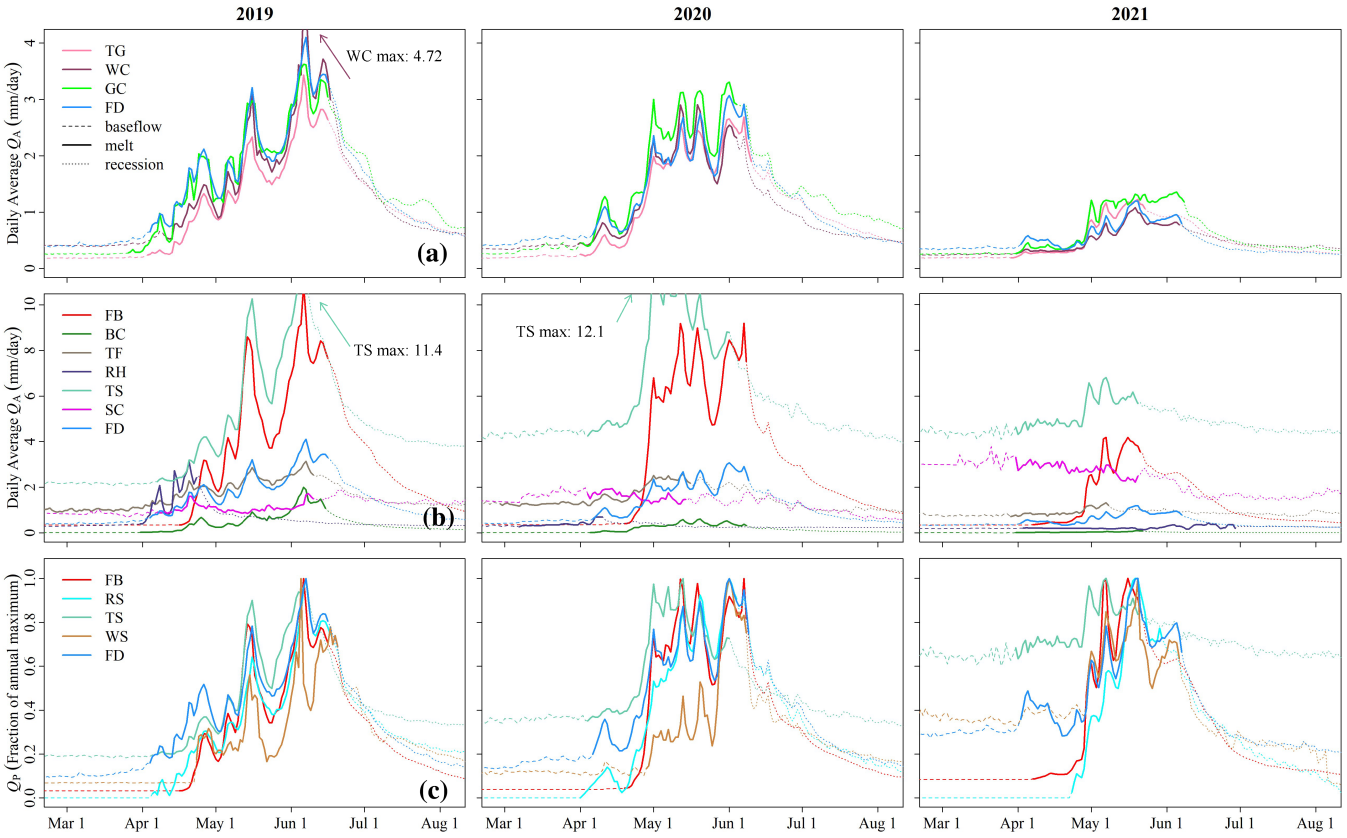

FIGURE 3 Area-normalized hydrographs (Q_A) for (row a) mainstem and (row b) tributary subcatchments during WY 2019 (Wet), 2020 (Moderate) and 2021 (Dry). Peak-normalized hydrographs (Q_P) for springs (RS, WS) and mainstem end members for comparison (row c). Site codes are defined in Table 1 and Figure 1. Line types denote the baseflow (dashed), snowmelt (solid) and recession (dotted) seasons. Additional years are provided in Figure S5.

Q_N values greater than 1 indicate higher flow per unit area relative to the watershed outlet, and positive (negative) slopes during the recession period indicate a more gradual (faster) snowmelt recession compared with the integrated watershed response.

During the baseflow period, spring-fed TS consistently had the highest Q_N and outlet-normalized median baseflow magnitudes (Table 2) of the non-spring monitoring sites (springs cannot be plotted in terms of Q_N) followed by SC and TF. Baseflow Q_N values in this complex increased from about 5 in a wet year to 11 in a dry year (Table 2, Figure 5). BC had the lowest Q_N baseflow by far (median baseflow 4%–13% of outlet), followed by TG (43%–57%) and RH (52%–67%), while FB and WC had similar Q_N baseflows to the outlet in most years (Table 2). At the start of the melt period, TS, SC and TF Q_N were all >1 with negative slopes, indicating elevated baseflow and a muted streamflow response to snowmelt compared with the outlet. In SC and TF, Q_N dropped below 1 during the melt period in moderate and wet years while TS consistently maintained the highest Q_N, although it also decreased over the melt period. In RH, Q_N exceeded 1 only in the early melt period in wet years and stayed below 1 later in the melt period in moderate and dry years. In FB, Q_N peaked at about 3 in wet years and 5 in dry years. During the recession period, TS had the steepest positive Q_N slope (monthly recession slope 177%–315% of outlet), followed by SC, TF, RH and GC. In contrast, FB had a steep negative Q_N recession slope across WYs, indicating much faster snowmelt recession rates than the integrated watershed response despite being the highest elevation subcatchment (Figure 5).

Finally, while tributaries and large springs presented a large range of seasonal streamflow patterns, these patterns could not be explained by typical watershed properties such as slope, elevation and surficial geology, contrasting with established controls on streamflow patterns in non-karst mountain watersheds. The scatterplots between hydrologic metrics and typical watershed properties revealed no significant trends across the watershed (Figure S3). Although median baseflow magnitude varied somewhat with average aspect, with the highest baseflow values occurring in west-southwest facing subcatchments (TF/SC/TS), these sites are also aligned with the bedding plane dip of underlying strata (Figure S1), which has been identified as a control on conduit orientation (Bahr, 2016) and is consistent with global understanding of structural influences on karst groundwater flow (Ford & Williams, 2007).

4 | DISCUSSION

4.1 | Karst controls on streamflow patterns

A major challenge in comparing annual streamflow patterns across mountain watersheds is separating the impact of climate and topographic influences from geologic controls (Tague & Grant, 2009).

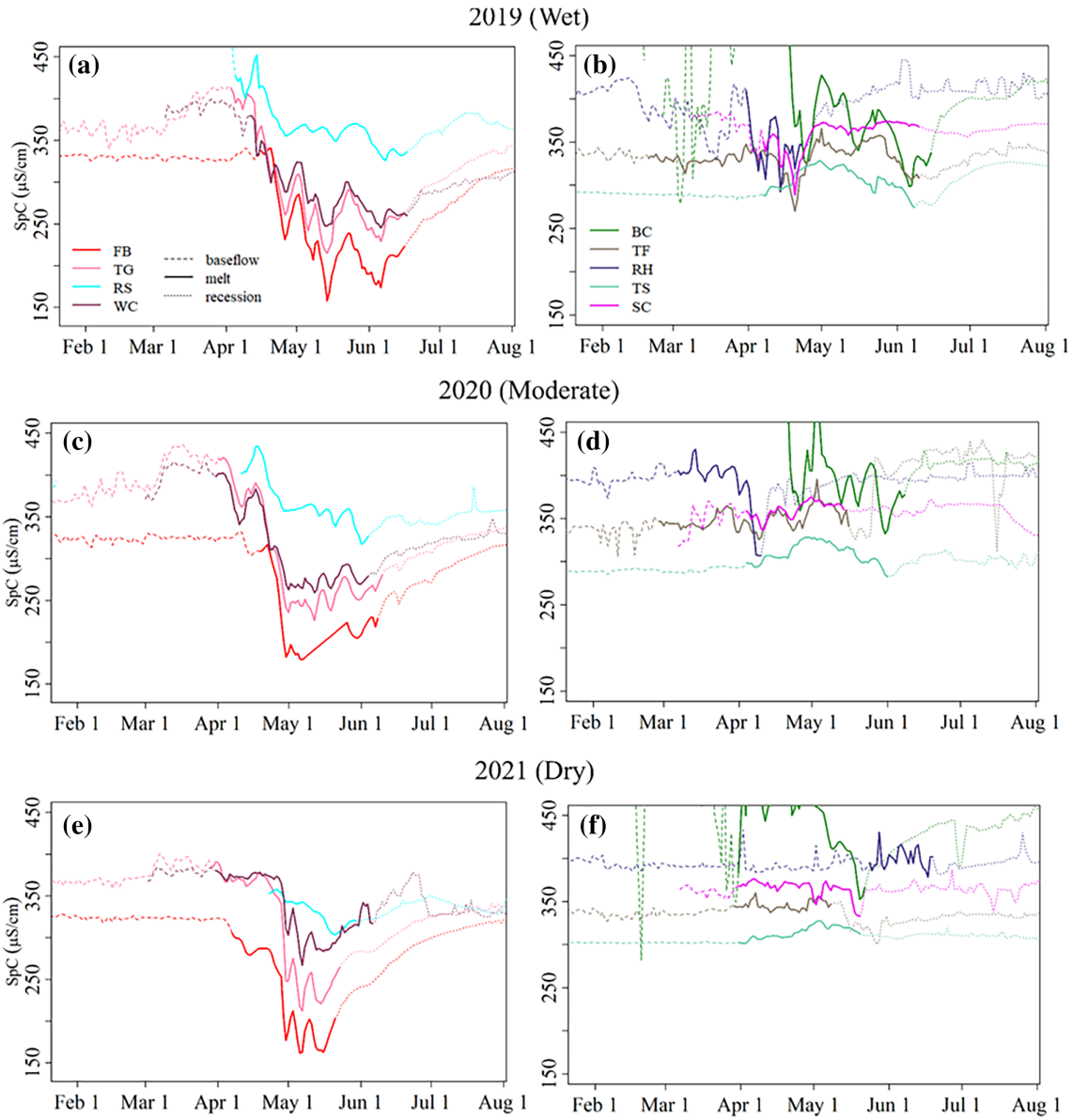

FIGURE 4 SpC at monitoring sites in a wet (WY 2019), moderate (WY 2020) and dry (WY 2021) year, where sites plotted in each column have distinct SpC patterns. Site codes are defined in Table 1 and Figure 1. Line types denote baseflow (dashed), snowmelt (solid) and recession (dotted) seasons.

Area- and outlet-normalized hydrographs exhibited substantial variability in the baseflow, snowmelt and recession periods across multiple subcatchments with similar climate forcing. One possible explanation for the elevated snowmelt signal in FB and TS (Figure 3) is variable precipitation inputs due to different orographic effects and snowmelt timing at different elevations and aspects (Xu et al., 2022). However, elevated runoff ratios are not observed in other high elevation subcatchments such as TG and BC. Overall, we did not observe typical effects of watershed properties (e.g., drainage area, elevation, annual precipitation, slope, aspect and antecedent baseflow) on streamflow metrics (Figure S3) found in non-karstic mountain watersheds such as those described by Kelleher et al. (2015) and Brooks et al. (2021). These findings corroborate recent studies suggesting that karst aquifer dynamics play a significant role in the fate and rerouting of snowmelt in the Logan River watershed (Neilson et al., 2018; Xu et al., 2022).

Although karst surface extent has been correlated with baseflow metrics in another carbonate-influenced watershed in the western United States (Tobin & Schwartz, 2020), no such relationships were observed here. This is likely the result of karst surface extent maps (Figure S1c) not providing insight regarding the three-dimensional complexity of the aquifer—including storage capacity, conduit network structure and groundwater flow directions that act as primary controls on outflow patterns. Karst area extent of RH and SC was both less than 50% due to widespread surficial deposits of the Wasatch Formation (Dover, 2007). However, this conglomerate is entirely underlain by carbonate strata, which are hydrologically influential but obscured in the surface extent variable.

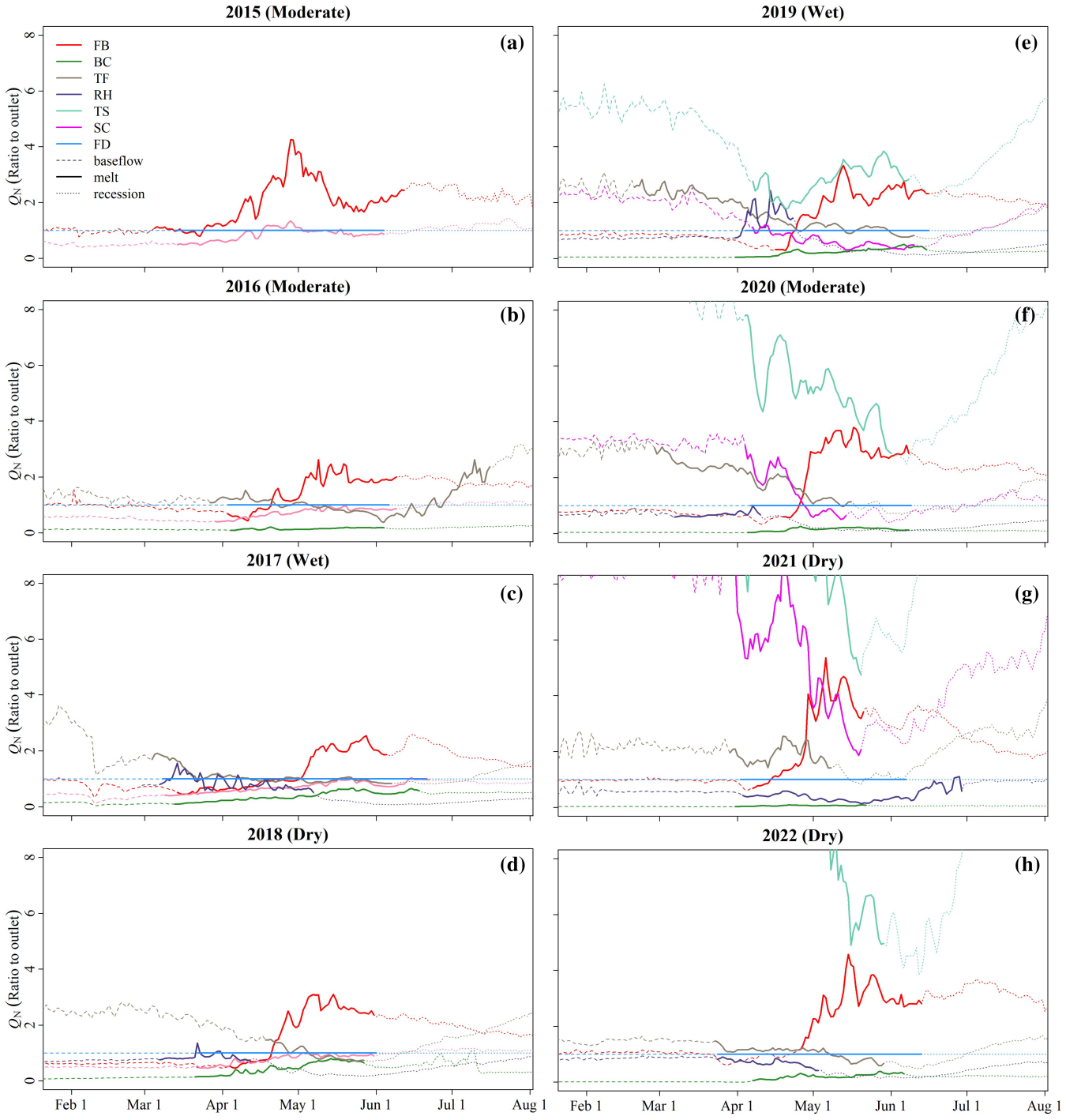

FIGURE 5 Average daily area-outlet normalized hydrographs (Q_N) for available sites in WY 2016–2022. Site codes are defined in Table 1 and Figure 1. Line types denote baseflow (dashed), snowmelt (solid) and recession (dotted) seasons.

4.2 | A conceptual model of subsurface controls on streamflow patterns in karst mountain watersheds

Area- and area-outlet normalized hydrographs and seasonal flow metrics provide an alternative approach for understanding karst watersheds in terms of dominant aquifer characteristics using streamflow data. Past studies of karst systems have proposed conceptual models and hypotheses for internal aquifer structural controls on streamflow patterns, which are summarized in Hartmann et al. (2014). These interpretations include a three-dimensional model of recharge, storage and transmission (Hobbs & Smart, 1986), linking recession or drawdown hydrograph characteristics to the conduit network distributions (Kresic, 2007), explanations of overflow spring triggers (Fleury et al., 2007) and recharge/discharge interactions between conduit

TABLE 2 Annual hydrologic metrics reported as ratios relative to the watershed outlet.

WY	FB	TG	BC	TF	RH	TS	SC	WC	GC
Outlet-normalized annual runoff ratio									
2015	1.39	0.69							
2016	1.23	0.68	0.13	1.53					
2017	1.23	0.64	0.32	1.41	0.49				
2018	1.14	0.63	0.25	1.92	0.70				
2019	1.69	0.61	0.18	1.65	0.65	4.04	1.40	0.87	0.91
2020	1.89	0.60	0.07	2.19	0.61	7.23	2.28	0.78	1.02
2021	1.86	0.68	0.04	2.44	0.73	11.80	6.90	0.81	1.04
2022	2.17	0.75	0.12	1.33	0.66	10.86		0.77	1.05
Outlet-normalized snowmelt runoff ratio									
2015	1.69	0.77							
2016	1.23	0.67	0.11	1.60					
2017	1.27	0.68	0.35	1.04	0.47				
2018	1.52	0.69	0.36	1.66	0.50				
2019	2.24	0.62	0.21	1.34	0.52	2.83	0.65	0.85	0.98
2020	2.64	0.69	0.11	1.83	0.47	4.91	1.02	0.78	1.13
2021	2.81	0.76	0.04	1.52	0.81	8.45	4.25	0.82	1.31
2022	3.10	0.77	0.16	0.92	0.39	7.13		0.80	1.11
Outlet-normalized monthly recession slope									
2015	1.79	0.78							
2016	1.93	0.73	0.16	0.05					
2017	2.23	1.03	0.63	0.95	0.65				
2018	2.69	0.87	0.62	0.41	0.14				
2019	2.41	0.73	0.43	0.54	0.65	2.86	0.11	1.06	0.87
2020	3.72	0.69	0.16	0.50	0.27	2.44	0.15	1.07	1.10
2021	3.93	1.02	0.11	0.69	0.27	1.77	1.29	0.67	1.45
2022	2.76	0.84	0.35	0.40	0.07	3.15		0.44	1.14
Outlet-normalized median baseflow magnitude									
2015	0.85	0.47							
2016	1.08	0.57	0.13	1.48					
2017	1.05	0.50	0.13	2.70					
2018	0.58	0.49	0.07	2.34	0.62				
2019	0.79	0.43	0.05	2.38	0.67	5.07	2.11	0.99	0.59
2020	0.69	0.43	0.04	2.53	0.64	8.19	3.30	0.79	0.64
2021	0.93	0.56	0.04	2.09	0.52	11.17	7.96	0.69	0.74
2022	1.03	0.57	0.01	1.46	0.81	15.00	9.43	0.77	0.82

Note: Non-normalized hydrologic metric values are available in Table S4. Empty cells indicate data was not available for those sites in those water years.

flow and matrix storage (Le Moine et al., 2007). These models form the basis for predictive streamflow model selection and parameterization (Rimmer & Salingar, 2006). However, the established considerations are most applicable to wells and individual springs and karst system structure becomes more apparent at larger (watershed) scales (Ford & Williams, 2007). The different streamflow and SpC patterns observed throughout the Logan River watershed in adjacent subcatchments with similar climate forcing suggest a need for an updated conceptual model that considers spatially distributed recharge and localized stratigraphic controls to address this gap.

The immense hydrologic heterogeneity across sites indicates some important additional differences in aquifer controls. We therefore propose a revised conceptual model of subsurface controls on streamflow patterns in karst mountain watersheds that, in addition to conduit and matrix flow, considers (1) inter-basin exchange directions of conduit flow (importing/exporting), (2) groundwater storage capacity and (3) the connectivity of storage to outflow springs or streams (Figure 6). We propose that these aquifer characteristics can be inferred from the area- and area-outlet normalized hydrograph patterns (Figure 5) and flow metrics (Table 2) described above. Note that

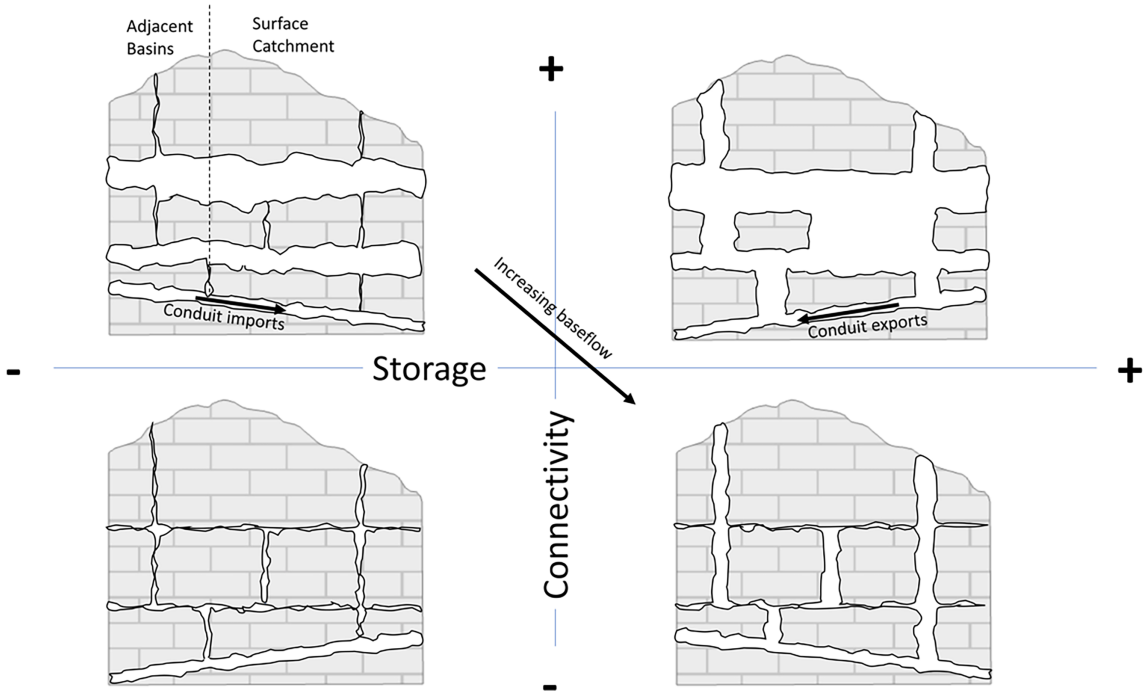

FIGURE 6 Proposed conceptual model to describe hydrogeologic distinctions between karstified subcatchments. Vertical conduit enlargement illustrates increased aquifer storage and horizontal conduit enlargement illustrates higher connectivity to spring outlets. The slope direction of the underlying drainage conduit represents groundwater import or export across topographic boundaries.

flow metric values henceforth refer to the ratio of metric values calculated at the subcatchment relative to the watershed outlet.

4.2.1 | Importing/exporting

The characterization of subcatchments as either importing or exporting groundwater flow is indicated by the annual and snowmelt period runoff ratios and the baseflow magnitude relative to the integrated watershed response as measured at the outlet. Importing systems are expected to have higher runoff ratios than the outlet (>1) due to a larger portion of SWIT (primarily snowmelt in mountain watersheds) going to discharge points and outlet-normalized cumulative melt discharge >1, while exporting systems should have lower runoff ratios and outlet-normalized cumulative melt discharge (<1). It should be noted that evapotranspiration may affect runoff values, making this distinction accurate, but not always sufficient for identifying importing systems. In the absence of SWIT information, similar distinctions may be made by comparing cumulative area-averaged discharge over the snowmelt period. However, comparing flow metrics directly rather than runoff ratios assumes uniform recharge depths, which may be unreasonable in mountain watersheds spanning a large elevation range. Variations in Q_N over the baseflow period may be attributed to piracy routes feeding water either into (elevated baseflow) or out of (reduced baseflow) each subcatchment (Hartmann et al., 2014; Liu et al., 2021) or to different conduits engaging at different times. Outlet-normalized median baseflow magnitude can help highlight systems with basinwide gains or losses, but this response is also influenced by aquifer connectivity and storage (see below).

4.2.2 | Connectivity

Connectivity refers here to the relative residence time or rate at which groundwater drains from the aquifer to spring outlets or streams. Connectivity is established by intersecting fracture and conduit networks and does not require an increase in total storage volume. The Q_N recession period characteristics point to drainage rates of the aquifer that can be associated with the degree of subcatchment connectivity. High connectivity is associated with rapid reductions in Q_A and low connectivity with a slower decrease in Q_A. Relative to the watershed outlet, this translates to a negative Q_N recession slope indicating high connectivity and a positive slope indicating low connectivity, as summarized by the outlet-normalized monthly recession rate or similar metric. Baseflow up to 6 months after any SWIT suggest that streamflow is sourced by matrix-level groundwater drainage or conduit storage with residence times of at least 8 months (Neilson et al., 2018). Associated low connectivity hydrologic indicators include baseflow Q_N >1 and a higher outlet-normalized runoff ratio the year after a wet year, indicating residence times longer than the prior-year water. This phenomenon is observed in the Temple Fork complex following the wet year of 2019. Connectivity may also vary seasonally and as a function of storage volume depending on the outflow rate of active connections, which may change with pressure head and aquifer

storage in complex ways. The paradoxical streamflow of RH in 2017 (Figure S4) suggests such aquifer complexity.

4.2.3 | Storage

Aquifer storage refers to the volumetric storage capacity available to be filled and drained. Given uniform aquifer connectivity, outlet-normalized baseflow values <1 indicate low-storage aquifers and >1 indicate high storage aquifers. However, because storage and connectivity are closely linked and difficult to separate, seasonal and interannual hydrologic variability can together point to the combined effect of storage and connectivity. Aquifers with large storage capacity and high connectivity may exhibit increased drainage rates during snowmelt associated with elevated Q_A peak flows, steeper recession slopes and baseflow magnitudes similar to the outlet. Alternatively, large storage aquifers with low connectivity may result in a Q_A peak flow similar to the outlet and elevated winter baseflows that stay elevated for a year or more after a wet year. A low-storage aquifer may have a similar Q_A peak to high storage/low connectivity aquifers, but Q_N stays ~1 over the baseflow period and Q_A may not remain elevated in years after a wet year, resulting in the highest outlet-normalized runoff ratios occurring during rather than following wet years.

The combination of dominant groundwater flow direction, connectivity and storage, each with two end members, results in eight possible end member hydrographs and relative metric values represented in terms of Q_A and Q_N in Figure 7.

4.2.4 | LRO subcatchment classifications

This proposed conceptual model was applied to the Logan River to illustrate its utility across diverse geologic and topographic settings. The highest elevation subcatchment FB exhibits high annual runoff ratios (1.14–2.17), likely indicating flow importing (Table 2). Extremely elevated peak flows and steep negative Q_N recession slopes (outlet-normalized monthly recession rate 1.79–3.93), particularly in dry years, indicate high connectivity, while low median baseflow magnitudes (0.69–1.08) suggest low storage. FB also had a substantial drop in SpC corresponding with streamflow rise, consistent with shorter residence time of karst conduit groundwater and direct surface runoff. Together, these hydrologic characteristics indicate more connected and larger diameter conduits with limited storage supply, characterizing FB as an importing aquifer with limited but highly connected storage (Figure 7a,c, top right panels). This interpretation is corroborated by the many mapped large karst conduit springs in FB (Neilson et al., 2018; Spangler, 2011), many of which go dry in fall or mid- to late-summer during dry years.

BC has the lowest Q_N across years and seasons and a very muted Q_N melt signal and peak flow, suggesting groundwater losses either to

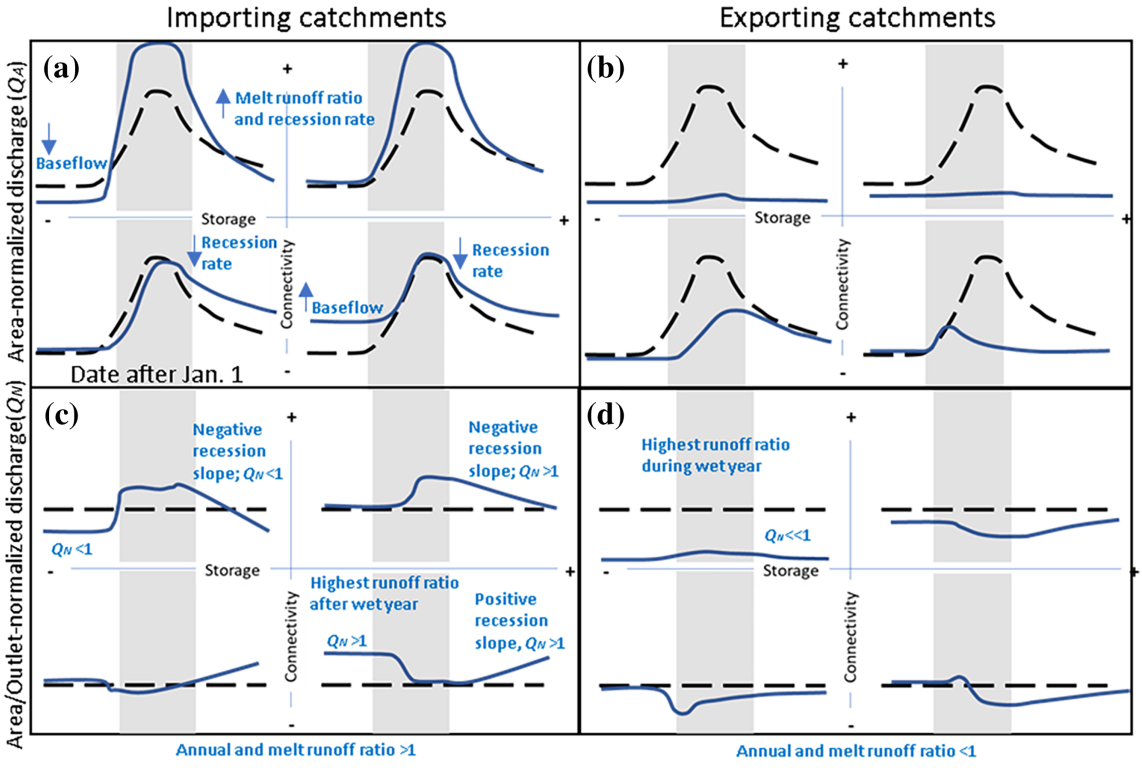

FIGURE 7 Archetype hydrographs for end member subcatchments (blue solid lines) compared to a watershed outlet (black dashed lines). Grey rectangles indicate the melt season. Panels (a) and (b) show area-normalized discharge (Q_A) for importing and exporting catchments, respectively. Panels (c) and (d) show area-outlet normalized discharge (Q_N). Noted outlet-normalized hydrologic metrics and Q_N features on plots highlight distinguishing characteristics used for aquifer characterization.

adjacent basins or the underlying bedrock (Figure 7). Its annual runoff ratio was highest in the wettest year (0.32) and melt runoff ratio never exceeded 0.36. Together, these findings indicate flow exporting. Because BC is largely non-responsive at the measurement site, little can be inferred about aquifer storage or connectivity from streamflow and SpC alone. However, taking a more holistic approach, we can use the conceptual model characteristics and metrics of adjacent subcatchments (e.g., FB is an adjacent importing watershed) and local knowledge to infer BC's characteristics. In late summer months, sections of BC go dry, despite having the largest topographic subcatchment area of all tributaries in the study area. Recent tracer studies attempting to map the northeastern portion of BC's subsurface connections have found large portions of the subcatchment exporting flow eastward to the Swan Creek watershed via large perennial springs that flow into Bear Lake with very short travel times (a few days) (L.E. Spangler, personal commun., March 2023). This suggests that BC is a large storage aquifer that is well connected—albeit not to the stream in its topographically defined subcatchment. However, in the western portion of the watershed (adjacent to FB), it is possible that some of the water being exported from BC is feeding the perennial springs in FB, again suggesting a large, well-connected storage aquifer.

In contrast with FB, the flatter recession slopes (Figure 2) and positive Q_N recession slope (Figure 5) of the Temple Fork complex and RH indicate less connected underlying structures (e.g., conduits, faults and fractures) and large karst groundwater stores that drain slowly. However, connectivity in TS appears to change over time as a function of storage. In wet WY 2017 and the following year, peak flow occurred at the same time as other sites, while in dry 2020 and 2021, flows peaked about a month earlier than other sites (May vs. June). This could indicate that when the storage is full, there is high connectivity via large conduits that maintain high flow rates. However, under low storage conditions (or when spring outflow exceeds snowmelt inflow rate), only low connectivity smaller conduits/matrix flow are activated.

The TS site had very high melt period Q_N values, a very steep positive Q_N recession slope and much higher cumulative melt period normalized discharge than other sites, particularly in dry years, indicating an importing aquifer with low but seasonally varying connectivity. SC and downstream TF exhibited similar but more muted streamflow patterns than TS, with high Q_N baseflow transitioning to ~1 during the snowmelt period and positive Q_N recession slopes (Figure 5). Aside from brief drops in SpC during wet-year snowmelt at SC and TF, likely from overland runoff, SpC at these sites stayed relatively stable and elevated. Together, these patterns suggest the activation of longer residence time subsurface storage into streamflow that may be due to longer or less connected flow paths and/or large fracture/matrix groundwater stores that feed the large Sawmill spring just upstream from TS. Therefore, all three subcatchments were characterized as importing aquifers with poor connectivity and large storage (Figure 7a,c, bottom right panels). This interpretation is supported by preliminary tracer studies indicating TS is fed in part by sinkholes about 3 km from the spring (personal comm. Larry Spangler). Interpreting the elevated baseflow Q_N of the Temple Fork complex as groundwater imports from adjacent basins is also consistent with karst conduits following bedding plane partings down-dip through the subcatchment (Figure S1b).

The RH subcatchment had the lowest Q_N values after BC—only exceeding 1 during peak flows in wet years (2017 and 2019)—and low annual (0.49–0.73) and snowmelt (0.39–0.81) runoff ratios, all suggesting an exporting aquifer. Unlike exporting from BC, a small melt response was observed in RH in wet years. However, peak flow timing occurred earlier than in other subcatchments, which may be partially attributed to lower catchment elevation (Figures 1 and S2). The runoff ratio in RH was higher in WY 2018 than in very wet 2017, indicating sufficient storage and low enough connectivity to maintain higher flows into the next year. As additional evidence, slightly positive Q_N recession slopes (slow drainage relative to outlet) point to low connectivity, and baseflows lower than the outlet per unit area (median baseflow magnitude 0.52–0.81) indicate moderate storage. RH was therefore characterized as exporting with moderate storage and low connectivity (Figure 7b,d, upper right panels; Table 2).

Along the mainstem, the Q_A (Figure 3) and Q_N plots illustrate the combined effects of the monitored tributaries and springs as well as other localized inputs established in previous studies (Neilson et al., 2018). In wetter years (2019), differences between the mainstem sites washed out. In drier years (2020, 2021), despite being closest to the outlet, GC had higher Q_A peak flows and recession flows and slightly faster recession rates compared with the other upstream mainstem sites (Figure 3). TG and WC (just upstream from WS) tracked FD well during snowmelt, but WC exhibited reduced recession rates, particularly in very dry years, indicating potential localized groundwater contributions. Looking at flow balances from different years, Neilson et al. (2018) found that the mainstem reach from WC to GC can be gaining or losing. This is likely dependent on localized karst influences along the river that either add or remove groundwater as a function of stage.

Finally, Q_P plots of the monitored springs (RS and WS) illustrate similar timing and recession rates of snowmelt period high flows, largely corresponding to high flow timing at FB and FD. However, in WY 2020, RS peaked in mid-May well before WS, more closely tracking the Q_P of FD and FB than WS. In very dry WY 2021, an early season snowmelt peak at the outlet was not observed at the springs or other upstream mainstem sites, which combined with the lack of SpC response (Figure 4) suggests isolated low-elevation flow contributions.

4.3 | Limitations and next steps

There remain many unknowns in karst hydrogeology that will require substantial monitoring and modelling resources to understand, such as the extent of aquifer recharge areas, dynamic piracy routes and timing of matrix–conduit exchange. The aim of this study was not to develop quantitative predictive models, but rather to use hydrologic timeseries based on readily measurable data to characterize controls on nested subcatchments and springs in a mountain watershed.

The only essential data requirement for this analysis is daily discharge for nested sites within a watershed, although SpC and simulated snowmelt timeseries data provided additional supporting evidence of dominant aquifer characteristics. As the seasonal responses were consistent for a given subcatchment across years, initial characterization could be performed with only one year of data, although additional years would improve the assessment.

The proposed approach provides a rapid assessment tool to evaluate relative streamflow sensitivity to snowpack and melt dynamics. Assessing streamflow sensitivity to snowmelt variability via improved understanding of groundwater controls in these hydrologic systems is critical (Godsey et al., 2014; Liu et al., 2021; Tague & Grant, 2009). Characterizing climate sensitivity typically requires long periods of record to perform trend analysis (Burn & Hag Elnur, 2002; Godsey et al., 2014) or the development and calibration of hydrologic models to evaluate climate scenarios (Arnoux et al., 2021; Chen et al., 2018; Hellwig et al., 2020). By linking observed snowmelt–discharge patterns to dominant aquifer characteristics according to our conceptual model, monitoring sites can be characterized in terms of relative climate sensitivity. For example, FB was characterized as a low storage, high connectivity aquifer, which would likely make it very sensitive to sustained drought and low snowpack conditions. In contrast, the Temple Fork complex sites were found to be underlain by a high storage, poorly connected aquifer, which should make them more resilient to climate variability, as indicated by high snowmelt and recession season Q_N values in TS and SC in very dry WY 2021 (Figure 5). These discharge-based assessments may be used to determine where in a watershed to focus more intensive monitoring or modelling studies, or to improve hydrologic model representation (Liu et al., 2021).

5 | CONCLUSION

Our study analysed several years of continuous snowmelt, streamflow and spring discharge data across 12 nested monitoring sites within a single karst mountain watershed. Hydrologic patterns across sites, years and seasons were linked to geologic influences, highlighting the significance of complex karst aquifer structure in driving snowmelt–discharge dynamics. A conceptual framework was proposed for characterizing aquifer dynamics of nested subcatchments and springs within a watershed based on commonly measured hydrologic timeseries in terms of conduit flow direction, aquifer connectivity and storage. Distinctions between study sites inferred through this framework were largely supported by previous hydrogeology studies. This framework may be used to improve understanding of dominant aquifer controls and climate sensitivity in other karst-influenced mountain watersheds in the absence of detailed hydrogeologic studies.

ACKNOWLEDGEMENTS

This work was supported by the U.S. National Science Foundation grants 2044051/2043363 and the Utah Water Research Laboratory, Utah State University. We thank Larry Spangler for his prior efforts and research insights regarding Logan Canyon that greatly improved the manuscript. We also thank Patrick Strong, Hyrum Tennant, Devon Hill, Abby Johnson, and all the Logan River Observatory technicians for their help collecting and compiling the data used within these analyses.

DATA AVAILABILITY STATEMENT

The data that support the findings of this study are openly available in Logan River Observatory at https://uwrl.usu.edu/lro/data.

ORCID

Belize Lane https://orcid.org/0000-0003-2331-7038
Tianfang Xu https://orcid.org/0000-0002-9565-9208
Bethany T. Neilson https://orcid.org/0000-0001-8829-5082

REFERENCES

Addor, N., Newman, A. J., Mizukami, N., & Clark, M. P. (2017). The CAMELS data set: Catchment attributes and meteorology for large-sample studies. *Hydrology and Earth System Sciences*, *21*(10), 5293–5313. https://doi.org/10.5194/hess-21-5293-2017

Arnoux, M., Brunner, P., Schaefli, B., Mott, R., Cochand, F., & Hunkeler, D. (2021). Low-flow behavior of alpine catchments with varying quaternary cover under current and future climatic conditions. *Journal of Hydrology*, *592*, 125591. https://doi.org/10.1016/j.jhydrol.2020.125591

Bahr, K. (2016). *Structural and lithological influences on the Tony Grove alpine karst system, Bear River Range, north-central Utah* (All Graduate Theses and Dissertations). Utah State University.

Barnhart, T. B., Molotch, N. P., Livneh, B., Harpold, A. A., Knowles, J. F., & Schneider, D. (2016). Snowmelt rate dictates streamflow. *Geophysical Research Letters*, *43*(15), 8006–8016. https://doi.org/10.1002/2016GL069690

Baudement, C., Arfib, B., Mazzilli, N., Jouves, J., Lamarque, T., & Guglielmi, Y. (2017). Groundwater management of a highly dynamic karst by assessing baseflow and quickflow with a rainfall-discharge model (Dardennes springs, SE France). *Bulletin de La Société Géologique de France*, *188*(6), 40. https://doi.org/10.1051/bsgf/2017203

Brooks, P. D., Gelderloos, A., Wolf, M. A., Jamison, L. R., Strong, C., Solomon, D. K., Bowen, G. J., Burian, S., Tai, X., Arens, S., Briefer, L., Kirkham, T., & Stewart, J. (2021). Groundwater-mediated memory of past climate controls water yield in snowmelt-dominated catchments. *Water Resources Research*, *57*(10), 1–15. https://doi.org/10.1029/2021WR030605

Burn, D. H., & Hag Elnur, M. A. (2002). Detection of hydrologic trends and variability. *Journal of Hydrology*, *255*(1–4), 107–122. https://doi.org/10.1016/S0022-1694(01)00514-5

Carlier, C., Wirth, S. B., Cochand, F., Hunkeler, D., & Brunner, P. (2018). Geology controls streamflow dynamics. *Journal of Hydrology*, *566*, 756–769. https://doi.org/10.1016/j.jhydrol.2018.08.069

Chang, Y., Hartmann, A., Liu, L., Jiang, G., & Wu, J. (2021). Identifying more realistic model structures by eElectrical conductivity observations of the karst spring. *Water Resources Research*, *57*(4), 1–18. https://doi.org/10.1029/2020WR028587

Chen, Z., Hartmann, A., Wagener, T., & Goldscheider, N. (2018). Dynamics of water fluxes and storages in an alpine karst catchment under current and potential future climate conditions. *Hydrology and Earth System Sciences*, *22*(7), 3807–3823. https://doi.org/10.5194/hess-22-3807-2018

Cochand, M., Christe, P., Ornstein, P., & Hunkeler, D. (2019). Groundwater storage in high alpine catchments and its contribution to streamflow. *Water Resources Research*, *55*(4), 2613–2630. https://doi.org/10.1029/2018WR022989

Curry, C. L., & Zwiers, F. W. (2018). Examining controls on peak annual streamflow and floods in the Fraser River Basin of British Columbia. *Hydrology and Earth System Sciences*, *22*(4), 2285–2309. https://doi.org/10.5194/hess-22-2285-2018

Deshmukh, A., & Singh, R. (2016). Physio-climatic controls on vulnerability of watersheds to climate and land use change across the U. S.: Controls on vulnerability. *Water Resources Research*, *52*(11), 8775–8793. https://doi.org/10.1002/2016WR019189

Dover, J. H. (2007). Geologic map of the Logan 30′ × 60′ quadrangle, Cache and Rich Counties, Utah, and Lincoln and Uinta Counties, Wyoming [digitized from the Dover (1995) USGS Map I-2210].

Fleury, P., Plagnes, V., & Bakalowicz, M. (2007). Modelling of the functioning of karst aquifers with a reservoir model: Application to Fontaine de Vaucluse (south of France). *Journal of Hydrology*, *345*(1–2), 38–49.

Ford, D., & Williams, P. (2007). *Karst hydrogeology and geomorphology*. John Wiley & Sons Ltd..

Godsey, S. E., Kirchner, J. W., & Tague, C. L. (2014). Effects of changes in winter snowpacks on summer low flows: Case studies in the Sierra Nevada, California, USA: Winter snowpacks and summer low flows. *Hydrological Processes*, *28*(19), 5048–5064. https://doi.org/10.1002/hyp.9943

Goldscheider, N., Meiman, J., Pronk, M., & Smart, C. (2008). Tracer tests in karst hydrogeology and speleology. *International Journal of Speleology*, *37*(1), 27–40.

Hartmann, A., Gleeson, T., Wada, Y., & Wagener, T. (2017). Enhanced groundwater recharge rates and altered recharge sensitivity to climate variability through subsurface heterogeneity. *Proceedings of the National Academy of Sciences*, *114*(11), 2842–2847.

Hartmann, A., Goldscheider, N., Wagener, T., Lange, J., & Weiler, M. (2014). Karst water resources in a changing world: Review of hydrological modeling approaches: Karst water resources prediction. *Reviews of Geophysics*, *52*(3), 218–242. https://doi.org/10.1002/2013RG000443

Hellwig, J., Graaf, I. E. M., Weiler, M., & Stahl, K. (2020). Large-scale assessment of delayed groundwater responses to drought. *Water Resources Research*, *56*(2), e2019WR025441. https://doi.org/10.1029/2019WR025441

Hobbs, S. L., & Smart, P. L. (1986). Characterization of carbonate aquifers: A conceptual base. *Proceedings of the 9th International Congress of Speleology*, Barcelona, 1, 43–46.

Horner, I., Branger, F., McMillan, H., Vannier, O., & Braud, I. (2020). Information content of snow hydrological signatures based on streamflow, precipitation and air temperature. *Hydrological Processes*, *34*(12), 2763–2779. https://doi.org/10.1002/hyp.13762

IPCC. (2015). In Core Writing Team, R. K. Pachauri, & L. A. Meyer (Eds.), *Climate change 2014: Synthesis report. contribution of working groups I, II and III to the fifth assessment report of the intergovernmental panel on climate change (Tech. Rep.)*. IPCC.

Jeannin, P. Y., & Sauter, M. (1998). Analysis of karst hydro-dynamic behaviour using global approaches: A review. *Bulletin d'Hydrogéologie (Neuchatel)*, *16*, 31–48.

Jefferson, A., Nolin, A., Lewis, S., & Tague, C. (2008). Hydrogeologic controls on streamflow sensitivity to climate variation. *Hydrological Processes*, *22*(22), 4371–4385. https://doi.org/10.1002/hyp.7041

Jódar, J., González-Ramón, A., Martos-Rosillo, S., Heredia, J., Herrera, C., Urrutia, J., Caballero, Y., Zabaleta, A., Antigüedad, I., Custodio, E., & Lambán, L. J. (2020). Snowmelt as a determinant factor in the hydrogeological behaviour of high mountain karst aquifers: The Garcés karst system, Central Pyrenees (Spain). *Science of the Total Environment*, *748*, 141363. https://doi.org/10.1016/j.scitotenv.2020.141363

Kelleher, C., Wagener, T., & McGlynn, B. (2015). Model-based analysis of the influence of catchment properties on hydrologic partitioning across five mountain headwater subcatchments. *Water Resources Research*, *51*, 4109–4136. https://doi.org/10.1002/2014WR016147

Kresic, N. (2007). Hydraulic methods. In N. Goldscheider & D. Drew (Eds.), *Methods in karst hydrogeology* (pp. 65–91). Taylor and Francis/Balkema.

Lachmar, T., Skyler, S., & Newell, D. (2021). Geochemical insights into groundwater movement in alpine karst, Bear River range, Utah, USA. *Hydrogeology Journal*, *29*(2), 687–701.

Le Moine, N., Andréassian, V., Perrin, C., & Michel, C. (2007). How can rainfall-runoff models handle intercatchment groundwater flows? Theoretical study based on 1040 French catchments. *Water Resources Research*, *43*, W06428. https://doi.org/10.1029/2006WR005608

Liu, Y., Wagener, T., & Hartmann, A. (2021). Assessing streamflow sensitivity to precipitation variability in karst-influenced catchments with unclosed water balances. *Water Resources Research*, *57*, e2020WR028598. https://doi.org/10.1029/2020WR028598

Neilson, B. T., Tennant, H., Stout, T. L., Miller, M. P., Gabor, R. S., Jameel, Y., Millington, M., Gelderloos, A., Bowen, G. J., & Brooks, P. D. (2018). Stream centric methods for determining groundwater contributions in karst mountain watersheds. *Water Resources Research*, *54*(9), 6708–6724. https://doi.org/10.1029/2018WR022664

Neilson, B. T., Tennant, H., Strong, P. A., & Horsburgh, J. S. (2021). Detailed streamflow data for understanding hydrologic responses in the Logan River observatory. *Hydrological Processes*, *35*(8), e14268. https://doi.org/10.1002/hyp.14268

Patterson, N. K., Lane, B. A., Sandoval-Solis, S., Pasternack, G. B., Yarnell, S. M., & Qiu, Y. (2020). A hydrologic feature detection algorithm to quantify seasonal components of flow regimes. *Journal of Hydrology*, *585*, 124787. https://doi.org/10.1016/j.jhydrol.2020.124787

Rimmer, A., & Salingar, Y. (2006). Modelling precipitation-streamflow processes in karst basin: The case of the Jordan River sources, Israel. *Journal of Hydrology*, *331*(3–4), 524–542.

Sauter, M. (1992). *Quantification and forecasting of regional groundwater flow and transport in a karst aquifer* (Vol. 13, p. 150). Tübinger Geowissenschaftlichen Abhandlungen, Reihe C.

Segura, C., Noone, D., Warren, D., Jones, J. A., Tenny, J., & Ganio, L. M. (2019). Climate, landforms, and geology affect baseflow sources in a mountain catchment. *Water Resources Research*, *55*(7), 5238–5254. https://doi.org/10.1029/2018WR023551

Somers, L. D., & McKenzie, J. M. (2020). A review of groundwater in high mountain environments. *WIREs Water*, *7*(6), 1–11. https://doi.org/10.1002/wat2.1475

Spangler, L. E. (2001). *Delineation of recharge in areas for karst springs in Logan canyon, Bear River range, northern Utah, paper presented at U. S. Geological Survey karst interest group*. U.S. Geological Survey Water Resources Investigations Report.

Spangler, L. E. (2011). *Karst hydrogeology of the Bear River range in the vicinity of the Logan River, northern Utah, paper presented at Geological Society of America Rocky Mountain—cordilleran section meeting*. U.S. Geological Survey.

Tague, C., & Grant, G. E. (2009). Groundwater dynamics mediate low-flow response to global warming in snow-dominated alpine regions: Groundwater dynamics and low-flow response. *Water Resources Research*, *45*(7) , 1–11. https://doi.org/10.1029/2008WR007179

Tarboton, D. G., & Luce, C. H. (1996). *Utah energy balance snow accumulation and melt model (UEB) in computer model technical description and users guide* (p. 64). Utah Water Research Laboratory and USDA Forest Service Intermountain Research Station.

Tobin, B. W., & Schwartz, B. F. (2020). Quantifying the role of karstic groundwater in a snowmelt-dominated hydrologic system. *Hydrological Processes*, *34*(16), 3439–3447. https://doi.org/10.1002/hyp.13833

Tyson, C., Longyang, Q., Neilson, B. T., Zeng, R., & Xu, T. (2023). Effects of meteorological forcing uncertainty on high-resolution snow modeling and streamflow prediction in a mountainous karst watershed. *Journal of Hydrology*, *619*, 129304.

Wang, Z., Chen, Q., Yan, Z., Luo, M., Zhou, H., & Liu, W. (2019). Method for identifying and estimating karst groundwater runoff components based on the frequency distributions of conductivity and discharge. *Water*, *11*(12), 2494. https://doi.org/10.3390/w11122494

Weary, D. J., & Doctor, D. H. (2014). *Karst in the United States: A digital map compilation and database: U.S. Geological Survey Open-File Report* 2014–1156. U.S. Geological Survey, p. 23. https://doi.org/10.3133/ofr20141156

White, W. B. (2002). Karst hydrology: Recent developments and open questions. *Engineering Geology*, *65*(2–3), 85–105.

Xu, T., Longyang, Q., Tyson, C., Zeng, R., & Neilson, B. T. (2022). Hybrid physically based and deep learning modeling of a snow dominated, mountainous, karst watershed. *Water Resources Research*, *58*(3) , 1–20. https://doi.org/10.1029/2021WR030993.

Xu, Z., Massei, N., Padilla, I., Hartmann, A., & Hu, B. (2018). Characterization, modeling, and remediation of karst in a changing environment. *Environmental Earth Sciences*, *77*(12), 476. https://doi.org/10.1007/s12665-018-7660-7

SUPPORTING INFORMATION

Additional supporting information can be found online in the Supporting Information section at the end of this article.

How to cite this article: Thurber, D., Lane, B., Xu, T., & Neilson, B. T. (2024). Dissolving the mystery of subsurface controls on snowmelt–discharge dynamics in karst mountain watersheds using hydrologic timeseries. *Hydrological Processes*, *38*(5), e15170. https://doi.org/10.1002/hyp.15170